Visualization of high dynamic range data in geosciences

Xiaoru Yuan [a,*], Yingchun Liu [b], Baoquan Chen [a],
David A. Yuen [c], Tomas Pergler [d]

[a] *Department of Computer Science & Engineering and Digital Technology Center,
University of Minnesota at Twin Cities, Minneapolis 55455, USA*
[b] *South China Sea Institute of Oceanology, Guangzhou 510301, China*
[c] *Department of Geology & Geophysics and Minnesota Supercomputing Institute,
University of Minnesota at Twin Cities, Minneapolis 55455, USA*
[d] *Department of Geophysics, Faculty of Mathematics and Physics, Charles University,
Prague 180 00, Czech Republic*

Abstract

High dynamic range data, the magnitudes of which span a wide range of scales, are pervasive in the geosciences. Simulations or measurements of many important geophysical processes, such as earthquakes, mantle temperature fluctuations, generate various high dynamic range data sets, in the form of volume or surface. Effective visualization of such datasets is vital for understanding such complex geophysical phenomena and poses a new challenge for both geoscientists and visualization scientists. We describe the general aspects of high dynamic range datasets in the geophysical sciences and provide three case studies of visualizing such data using the techniques we have developed recently. They include: (1) visualizing the Earth's mantle structures using high dynamic volume volume visualization (HDR VolVis); (2) visualizing surface ruptures during earth quakes using an interference-based method; (3) visualizing tsunami waves again using interference-based method. To improve the performance of visualizing these datasets, which are usually large in size, modern commodity graphics hardware are leveraged to provide simultaneously efficient simulation and visualization.
© 2007 Elsevier B.V. All rights reserved.

1. Introduction

The magnitudes of most data in the geosciences span a wide range of scales. These high dynamic range data exist in the form of volume or surface and can be obtained from either simulation or measurement of many important geophysical processes, such as mantle temperature fluctuations and earthquakes. It is vital, and in the same time challenging, to effectively visualize such datasets for understanding these inherently complex geophysical phenomena.

The dynamic range is defined as the ratio between the smallest distinguishable increment and the largest

---

* Corresponding author.
E-mail addresses: xyuan@cs.umn.edu (X. Yuan),
liuyingch@mails.gucas.ac.cn (Y. Liu), baoquan@cs.umn.edu
(B. Chen), daveyuen@gmail.com (D.A. Yuen).

possible span of the values of a variable quantity in numerous fields as expressed in Eq. (1).

$$D = \frac{V_{max} - V_{min}}{d} \tag{1}$$

where V_{max} and V_{min} are the largest and smallest possible value of variable V, respectively, and d is the smallest increment of V. The value of d could either be the limit of the measurement device or the baseline noise for measured data, or the finest precision in the computation. Data with large variation or high dynamic range are common both in simulations and real measurements.

To gain a better understanding of high dynamic range data and the challenge of visualizing them, let us look at the optical properties of scenes from the real world, which often have a wide range of colors and intensities. In color science, dynamic range is defined as the ratio between the maximum and the minimum non-zero tonal values in an image. Algorithms have been developed for capturing both photographs (Debevec and Malik, 1997) and videos (Kang et al., 2003) with a high dynamic range of over 10^5. The resulting image or video are stored in floating-point format or in special coding scheme such as RGBE/XYZE, OpenEXR, LogLuv and so on. On the display or storage side, the 8-bits-per-channel image representation is popular. The dynamic range of most available electronic display devices have no more than two orders of magnitude. Paper or other printing media have much more limited dynamic range. Tone mapping operators (Durand and Dorsey, 2002; Fattal et al., 2002; Larson et al., 1997; Pattanaik et al., 1998; Reinhard et al., 2002; Tumblin and Rushmeier, 1993; Tumblin and Turk, 1999) have been developed to bridge the gap between high dynamic images and low dynamic range display devices. In general, two types of tone reproduction operators have been proposed to convert high dynamic range data to displayable low dynamic range data while preserving most of the data features: global (spatially uniform) operators and local (spatially varying) operators (Devlin et al., 2002). Global operators apply the same function to every pixel throughout

an image. One global operator may depend upon the contents of the image as a whole, and the same transformation is applied to every pixel. The logarithmic scaling is considered as a global tone operator popularly used in many practice. Conversely, local operators apply a different scaling to different parts of an image. With the development of commodity graphics hardware, many tone mapping algorithms can be accelerated on graphics hardware (Goodnight et al., 2003). Recently, a high dynamic range display device has been developed (Seetzen et al., 2004) based on a combination of an liquid crystal display (LCD) panel and a digital light processing (DLP) projector. Nevertheless, tone mapping is still necessary, when the dynamic range of the data is higher than that of the high dynamic range display device, which is very often the case.

Many geophysical properties have a wide dynamical range, typically going up to one thousand or beyond as listed in Table 1. Tsunami wave heights can span between 10 cm to 50 m. In fault ruptures, the dynamical range of the displacement can span more a thousand times ranging between slow creep and supersonic speed. The range of frequency in seismic waves also can range from 10 Hz associated with body waves to 0.001 Hz in free oscillations. The speed in mantle convection can range from 0.1 cm per year in transient uplifts to 100 cm per year as in fast mantle plumes. The energy released in one seismic events could be varying dramatically. Microearthquakes with Richter magnitude less then 2.0 are not commonly felt by people and can not be recorded on local seismographs. Great earthquakes, such as the Sumatra-Andaman earthquake on December 26, 2004 causing the Asian Tsunami has magnitude as high as 9.3. The energy released in such events is multiple billions times more than that the microearthquakes does. Due to the large span of the released energy in earthquakes of different magnitude, scales in logarithm have been used to measure the intensity of the earthquakes. However, for many cases, simply using logarithmic scale does not always work. The compression is not adapted to the characteristics of the individual data and important features may lost during the conversion.

Table 1
List of high dynamic range variables in geosciences

Variable	Minimum value	Maximum value	Dynamic range
Rupture displacement	Centimeters	10 m	10^3
Sea wave height	1 cm	10 m	10^3
Mantle temperature fluctuation	0.1 K	1000 K	10^4
Seismic wave frequency	0.1 s	Hours	10^4
Mantle convection	0.1 cm per year	1 m per year	10^3
Dynamical pressure	0.1 MPa	100 MPa	10^3

In the next section, we introduce techniques that we have developed recently for tackling this problem.

2. Visualization techniques for high dynamic range data

High dynamic range data bearing abundant features need special treatment during the visualization and the display stage to avoid losing subtle but important features due to the dynamic range compression. As we have discussed in the previous section, although high dynamic range data are not unusual and have existed for quite a long time in scientific research domains, visualization of such high dynamic data has not been investigated thoroughly until recently (Yuan et al., 2005, 2006). In this section, we discuss two visualization methods developed for volumetric and surface data, respectively. Examples of these visualization methods are demonstrated and discussed in Section 3.

2.1. High dynamic range surface visualization

In the geosciences, it is not uncommon to visualize physical quantities associated with a surface. For example, in the tsunami hazard study, the wave height on the ocean surface and its variation when the wave approaches the coast are critical for evaluating the impact of hypothetical tsunamis. In such occasions, the scalar value associated with the surface could have high dynamic range.

Here, we briefly describe one visualization method we have developed (Yuan et al., 2007), which is inspired by interference phenomena (Williamson and Cummins, 1983). Two examples of using this method are demonstrated in the next section.

In this visualization method, high dynamic range scalar value of the surface is rendered according to the intensity modulation of the interference pattern to capture subtle local quantitative variation. Color mapping can be used together with the intensity modulation to further enhance the visualization. The interference-based visualization method is not intended to exactly simulate the natural interference phenomena, but to use the interference patterns for visualizing high dynamic range scalar values on surfaces.

Briefly speaking, interference is the interaction between two or more waves, when they pass the same point. Constructive interference occurs when the waves add in phase, producing a larger peak than either wave alone: whereas destructive interference occurs when waves add out of phase, producing smaller peaks than one of the waves by itself.

Consider the interference between two coherent monochromatic waves with wave functions ψ_1 and ψ_2,

$$\psi_n = \sqrt{I_n}\mathrm{e}^{\mathrm{i}(\mathbf{kr_n}-\omega t+\varepsilon_n)} \tag{2}$$

where I is irradiance, $\mathbf{k}$ the propagation vector, $\mathbf{r}$ the position vector, ω the angular temporal frequency and ε is the initial phase ($n = 1, 2$). If they interfere coherently, then

$$\psi = \psi_1 + \psi_2 = \sqrt{I_1}\mathrm{e}^{\mathrm{i}(\mathbf{kr_1}-\omega t+\varepsilon_1)} + \sqrt{I_2}\mathrm{e}^{\mathrm{i}(\mathbf{kr_2}-\omega t+\varepsilon_2)} \tag{3}$$

if $I_1 = I_2 = I_0$ the interference intensity can be expressed as

$$I = 2I_0(1 + \cos\delta) = 2I_0\cos^2\delta/2 \tag{4}$$

where

$$\delta = \mathbf{k}(\mathbf{r}_1 - \mathbf{r}_2) + (\varepsilon_1 - \varepsilon_2) = \mathbf{k}\Delta\mathbf{r} + \Delta\varepsilon \tag{5}$$

where δ is the phase difference arising from path length difference if the initial phases are same. Constructive interference occurs when the phase difference between the two waves is an even integer multiple of π. Destructive interference occurs when the phase difference between the two waves is an odd integer multiple of π.

In this interference-based visualization method, light path differences are defined by the surface values to be visualized. These path differences then modulate the lighting intensity to generate the interference patterns which are then used to convey data values. Assume at one point that the movement or deformation is $\mathbf{d}$. Two coherent light waves travel at a distance proportional to $\mathbf{d}$.

The phase difference are defined as:

$$\delta = 2\pi\nu\mathbf{d} \tag{6}$$

where ν is the frequency parameter used to control the frequency of the interference pattern. Then the interference intensity I will vary according to $(1 + \cos 2\pi\nu\mathbf{d})$. Since the modulation term is a trigonometric function with a period of 2π, each pair of peaks in the interference pattern indicates a difference of $1/\nu$ in d. We will refer to the value $1/\nu$ as the resolution of the subsequent interference-based visualization.

The visualization can be straightforwardly implemented. To improve the efficiency, we leverage commodity graphics hardware (Yuan et al., 2007). Fig. 1 illustrates the results of a two-step visualization. In the first step, multiple data propensities can be rendered simultaneously with the result of each stored in a separate texture component. The current multiple render targets
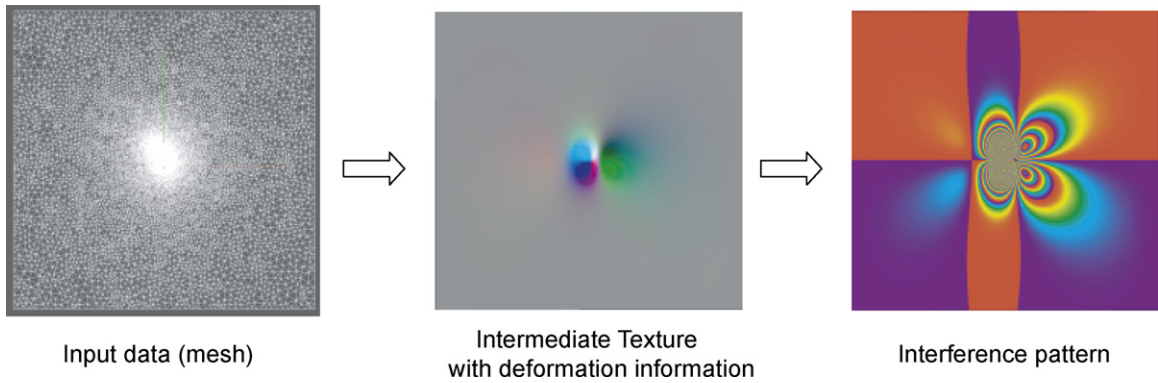
Fig. 1. Two-step interference-based visualization.

(MRT) features enables us to simultaneously render up to four textures in a single pass. We use floating point textures to store the intermediate results. In the second step, users choose the surface properties they wish to visualize. The visualization program computes the interference patterns based on the above equations, using a graphics hardware application programming interface (API) feature called fragment shader together with a color lookup table.

2.2. High dynamic range volume visualization

Many geophysical simulations produce large volumetric data with high dynamic range values. In this subsection, we briefly describe the high dynamic range volume visualization framework *HDR VolVis* developed by Yuan et al. (2005, 2006).

Geophysical properties of simulation data are normally stored in 32- or 16-bit floating-point precision. Quantizing them to 8-bit scalar values to fit in the texture-based volume rendering (Rezk-Salama et al., 2000) on currently available commodity graphics hardware will severely degrade the data quality and inevitably lose subtle, but important details, especially in multiscale phenomena.

As suggested in Yuan et al. (2005, 2006), it is desirable to have high precision alpha (transparency) compositing to preserve detailed structures residing in the data, when small opacity of each volume slices are desirable to minimize occlusions and to better reveal the internal volumetric structures.

The HDR VolVis framework performs high precision volume compositing (during the rendering, computing with floating numerical precision instead of only fixed one-byte precision), which is followed by dynamic tone mapping to preserve details on regular display devices. The basic pipeline of the HDR VolVis framework is illustrated in Fig. 2. The input of the HDR VolVis framework is high dynamic range data with both high spatial and intensity resolutions. In the first step, high dynamic range transfer functions are applied to volume value of the entire intensity range. An interface with non-linear magnification of intensity range and logarithmic scaling of color/opacity range is designed to facilitate high dynamic range transfer function specification. In the next stage, high precision composition is performed to retain the volumetric details. The output is in high dynamic range image format. Such output image is then displayed on regular display with tone mapping, a procedure to minimize the loss of the computed details.
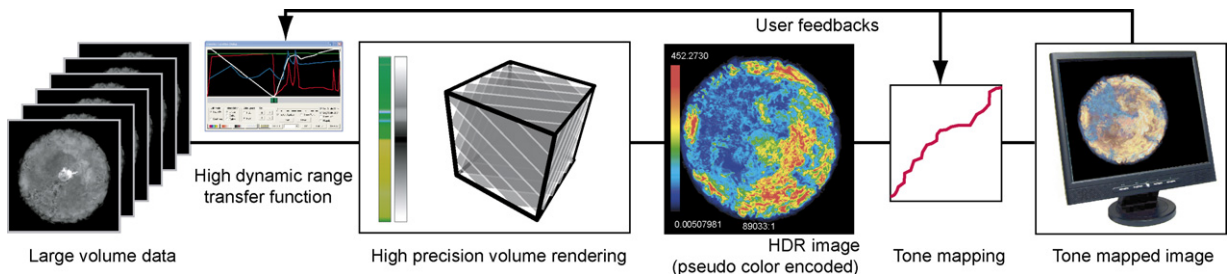

Fig. 2. Pipeline of HDR VolVis. The input is a scalar 3-D volume with high precision and/or high resolution. The intermediate output is a high dynamic range image after high precision compositing. By applying a tone mapping operator, the final result can be displayed on a regular display device with low dynamic range.

A user can adjust the tone mapping function for the final display to enhance selected features. By further leveraging modern commodity graphics hardware and out-of-core acceleration Farias and Silva (2001), the HDR VolVis framework is capable of producing interactive visualization of large volume data.

3. Case studies

3.1. Case I: Visualizing tsunami wave height

In this case study, we visualize the height of simulated tsunami waves generated by tsunamogenic earthquake in South China Sea (Liu et al., 2007; Yuan et al., 2007).

A tsunami is a series of waves generated, when a large body of water is rapidly displaced on a massive scale. Tsunamis are often caused by the submarine earthquakes. A tsunami has a much smaller amplitude offshore, and a very long wavelength, hundreds of kilometers, which is why they generally pass unnoticed at sea, forming only a passing "hump" in the ocean. As the tsunami wave approaches, the shallow waters of shore, its wavelength decreases rapidly, causing the water to pile up to form tremendous crests. With these characteristics, the simulated tsunami waves have very low wave height in the deep water region and very large wave height values near the coastal regions, which create data sets with typically a high dynamic range.

The field area of this work is the South China Sea. The simulated tsunami wave height can then be combined with the computed earthquake probability to give the prediction of tsunami hazard on the cities of the mainland China coast (Liu et al., 2007).

The trenches of the South China Sea stretch in a north to south direction, from south of the Taiwan island, passing the west of Luzon and extending to the west of
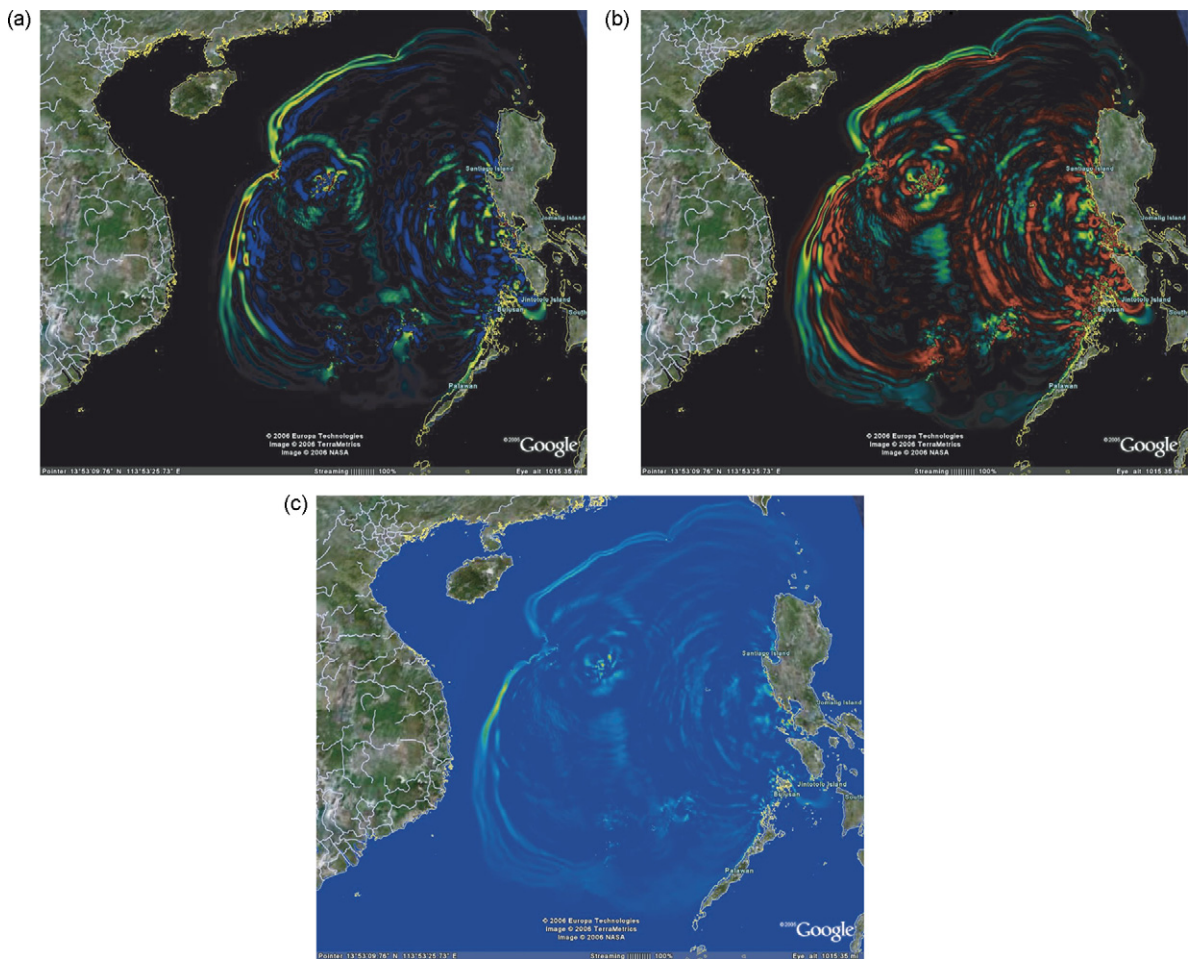

Fig. 3. Visualization of wave height generated by tsunamogenic earthquake in South China Sea. (a) Color mapped to each period of the interference pattern, (b) color mapped to the whole data range and then modulated by interference pattern and (c) direct color map.

Mindanao. The sea-bottom topography of the Manila trench is very complicated. The large variation of water depth and sea-bottom topography indicates the possibility tsunamogenic earthquake in this particular region. The Manila trench is the fault-graben trough dominated by normal fault, on the boundary of the graben system of the South China Sea and the Philippine island-arc fault-fold system. The western part of the Manila trench fault zone is formed by the steepened fault and the depression of Central oceanic basin of the South China Sea. In terms of the fault movement, Manila trench fault zone has now been recognized as the most likely to generate tsunamis in the South China Sea.

Based on this reasoning, a simulation on the sea water wave height in that region has been conducted. As shown in Fig. 3(a), we apply the interference-based visualization to the wave height data computed. The wave height is stored in its absolute value. A color texture is then mapped to each period of the interference pattern. The regions with denser interference fringes are associated with higher wave height and in larger danger of tsunami. Fig. 3(b) illustrates a color texture mapped to the whole data range and then modulated by interference pattern. Fig. 3(c) depicts the image using a direct color mapping without any enhancement from the interference pattern.
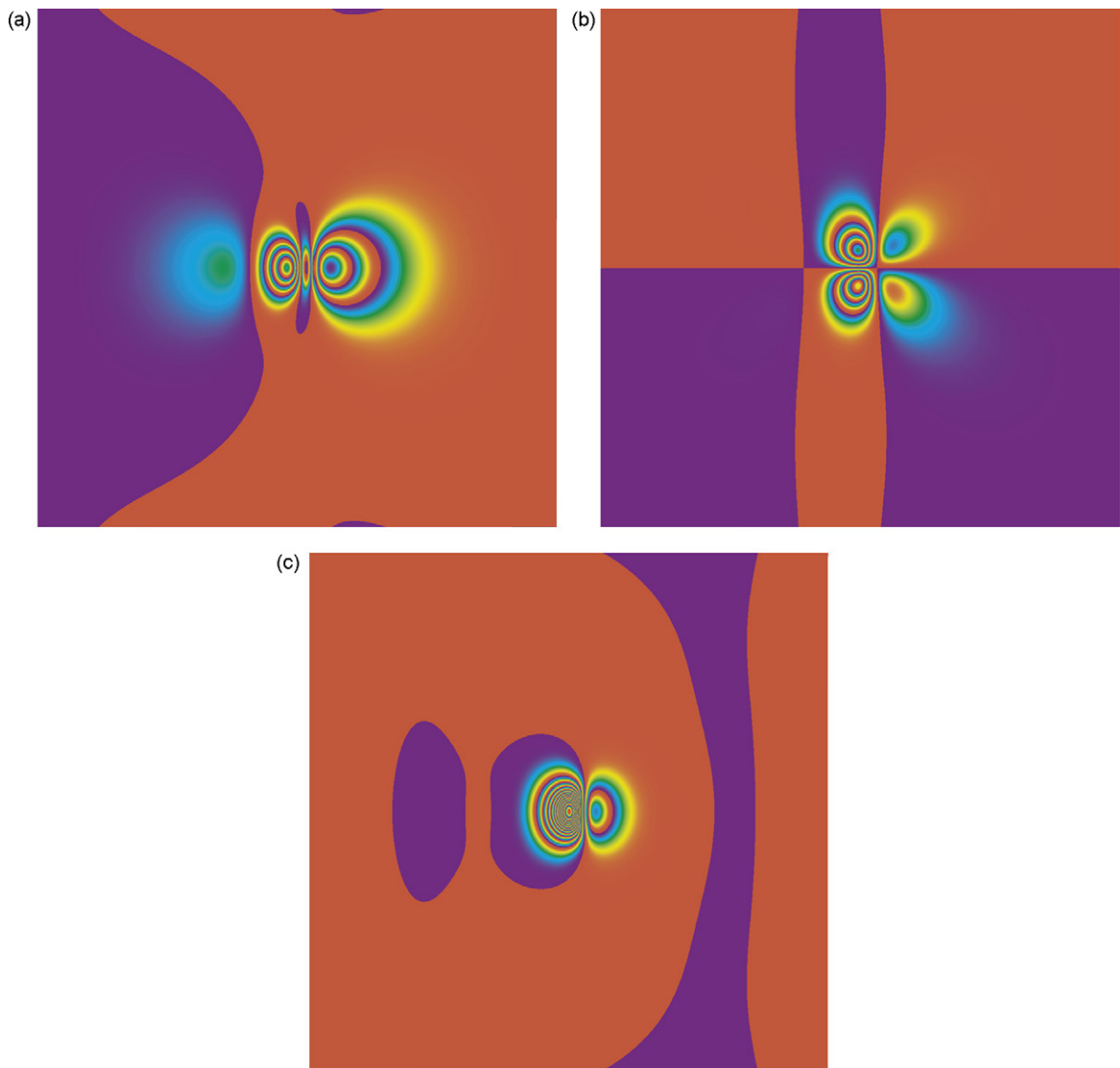

Fig. 4. (a) *x* Component, (b) *y* component and (c) *z* component of the fault deformation simulated by a hybrid 3-D numerical model, which employs a 2-D finite-element and a spectral method in one direction. The interference-based visualization has a v value of 8.
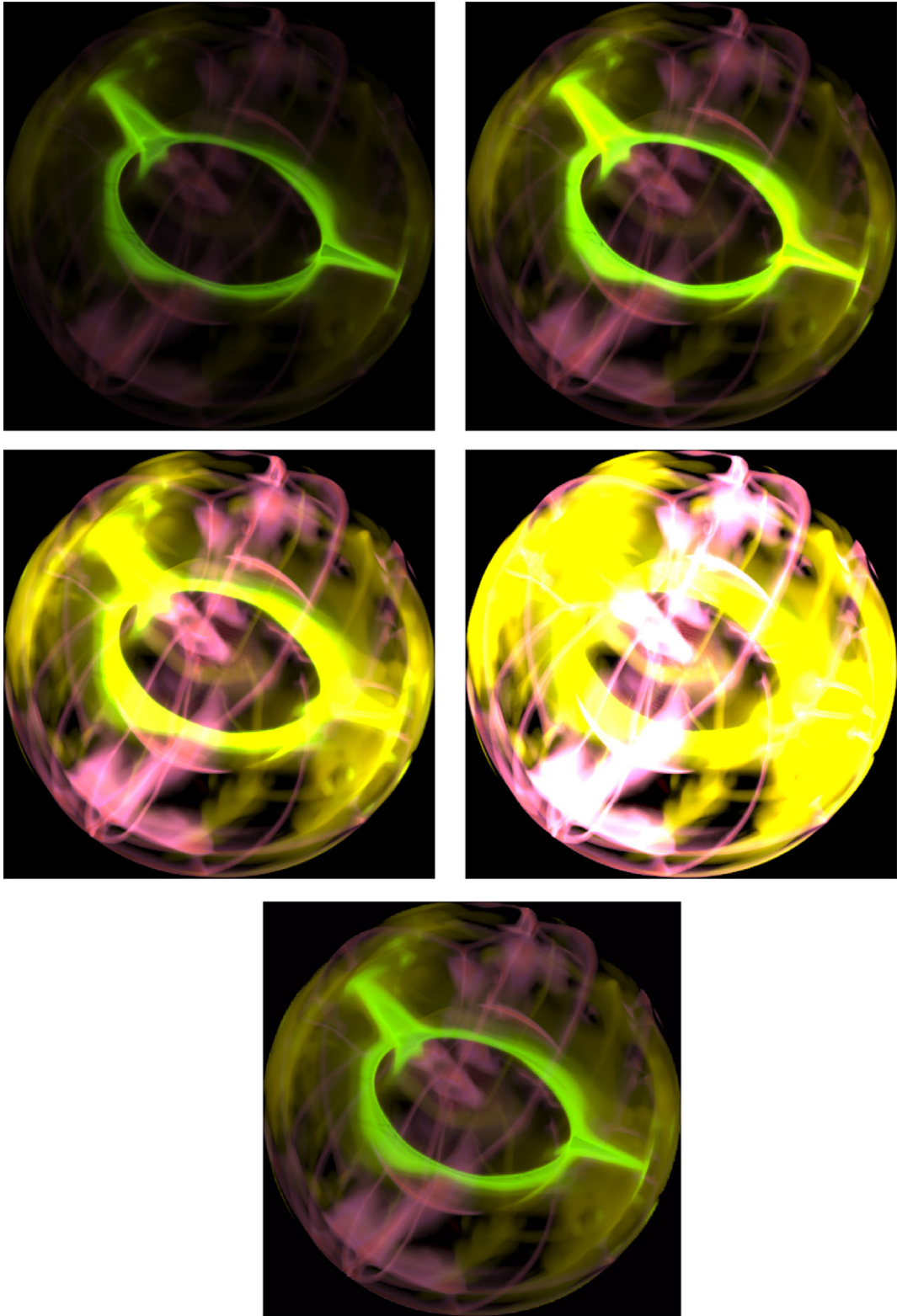
Fig. 5. High dynamic visualization of the Earth's mantle convection in 3-D sphere. The top four images are the rendered results at different exposures. The bottom image is a tone mapped result of the high dynamic rendering.

3.2. Case II: Visualizing surface deformation from earthquakes

In the second case, we visualize the surface deformation from earthquakes based on a hybrid numerical method that combines from finite element discretization in 2-D together with a Fourier series decomposition in the third dimension. The computation result represents the elastic displacements on the 2-D fault.

The domain of the subduction model has size of $1000\,\text{km} \times 1000\,\text{km} \times 600\,\text{km}$. The fault strike is $0°$, the dip angle is $6°$ and the rake angle is $-90°$. The fault is in depth of $50\,\text{km}$ and amplitude is $10\,\text{m}$, its length in y-coordinate is $100\,\text{km}$ and its second dimension is $50\,\text{km}$.

In Fig. 4, we visualize the computational results, using the interference patterns. A color map is mapped to each period of the interference pattern. Fig. 4(a)–(c) show the x, y and z components of the fault deformation fields, respectively. The interference-based visualization has a v value of 8. Note the boundary between color blue and red is due to the two ends of the texture where we used have different colors. If a cyclic texture is used, there will not be any sharp color boundaries.

3.3. Case III: Visualizing the earth's mantle convection

Mantle convection is now recognized to be the driving mechanism of plate tectonics. It governs the earth's thermal and chemical evolution and involves both thermal and compositional transport. Mantle-convection processes act over multiple scales because of the many nonlinearities in the system, such as from rheology and sharp compositional gradients. There are many grand challenge problems in mantle convection requiring the combined expertise of geophysics, information technology and fluid dynamics. Visualization and advanced data analysis is crucial for interpreting the results.

The volumetric data we visualize in this part is generated by a spectral spherical convection code (Monnereau and Yuen, 2002). The original spherical coordinates are converted to Cartesian coordinates by placing the sphere in a box and doing a linear interpolation. The final size of the mantle convection data is $513 \times 513 \times 513$ grid points.

In Fig. 5, we show the four images all based on one single high dynamic range volume visualization output, which is a high dynamic range image with all details preserved. Similar to change the exposure time in photograph, we can applied different exposure parameters to the rendered HDR image and obtain the first four images in the figure. We note in the dark and bright images, different features can be revealed, respectively. We can also render a single image (the bottom image of Fig. 5) by applying the tone mapping operators for showing on regular display devices.

4. Concluding remarks

Data with a high dynamic range can be found throughout the geosciences. In this article, we discuss methods, interference-based visualization and HDR VolVis, which have been recently developed for visualizing high dynamic range data in surface and volume format, respectively. Three high dynamic range data sets generated in geophysical simulations we have visualized.

Although in the case studies here, we have visualized only the results from numerical modeling, there are also many measured data with properties having a high dynamic range. It would also be interesting to apply these visualization methods to these data, such as found in geodesy.

With the capability facilitated by the high dynamic range visualization methods, we should encourage scientists in the geoscience community to pursue even larger scale and higher precision simulation to capture important, yet subtle physical properties that may lead to new discovery in areas such as tsunami modeling and mantle dynamics.

References

Debevec, P.E., Malik, J., 1997. Recovering high dynamic range radiance maps from photographs. In: SIGGRAPH '97, pp. 369–378.

Devlin, K., Chalmers, A., Wilkie, A., Purgathofer, W., 2002. STAR: tone reproduction and physically based spectral rendering. In: Eurographics'02, pp. 101–123.

Durand, F., Dorsey, J., 2002. Fast bilateral filtering for the display of high-dynamic-range images. In: SIGGRAPH '02, pp. 257–266.

Farias, R., Silva, C.T., 2001. Out-of-core rendering of large, unstructured grids. IEEE Comput. Graph. Appl. 21 (4), 42–50.

Fattal, R., Lischinski, D., Werman, M., 2002. Gradient domain high dynamic range compression. In: SIGGRAPH '02, pp. 249–256.

Goodnight, N., Wang, R., Woolley, C., Humphreys, G., 2003. Interactive time-dependent tone mapping using programmable graphics hardware. In: Proc. of the 14th Eurographics Symposium on Rendering, pp. 26–37.

Kang, S.B., Uyttendaele, M., Winder, S., Szeliski, R., 2003. High dynamic range video. ACM Trans. Graph. 22 (3), 319–325.

Larson, G.W., Rushmeier, H., Piatko, C., 1997. A visibility matching tone reproduction operator for high dynamic range scenes. IEEE Trans. Visual. Comput. Graph. 3 (4), 291–306.

Liu, Y., Santos, A., Wang, S.M., Shi, Y., Liu, H., Yuen, D.A., 2007. Tsunami hazards from potential earthquakes along south china coast. Phys. Earth Planet. Interiors (PEPI). Elsevier, 2007, in press.

Monnereau, M., Yuen, D., 2002. How flat is the lower-mantle temperature gradient? Earth Planet. Sci. Lett. 202, 171–183.

Pattanaik, S.N., Ferwerda, J.A., Fairchild, M.D., Greenberg, D.P., 1998. A multiscale model of adaptation and spatial vision for realistic image display. In: SIGGRAPH '98, pp. 287–298.

Reinhard, E., Stark, M., Shirley, P., Ferwerda, J., 2002. Photographic tone reproduction for digital images. In: SIGGRAPH '02, pp. 267–276.

Rezk-Salama, C., Engel, K., Bauer, M., Greiner, G., Ertl, T., 2000. Interactive volume rendering on standard PC graphics hardware using multi-textures and multi-stage rasterization. In: Proc. of the SIGGRAPH/EUROGRAPHICS workshop on Graphics Hardware, pp. 109–118.

Seetzen, H., Heidrich, W., Stuerzlinger, W., Ward, G., Whitehead, L., Trentacoste, M., Ghosh, A., Vorozcovs, A., 2004. High dynamic range display systems. ACM Trans. Graph. 23 (3), 760–768.

Tumblin, J., Rushmeier, H., 1993. Tone reproduction for realistic images. IEEE Comput. Graph. Appl. 13 (6), 42–48.

Tumblin, J., Turk, G., 1999. LCIS: a boundary hierarchy for detail-preserving contrast reduction. In: SIGGRAPH '99, pp. 83–90.

Williamson, S.J., Cummins, H.Z., February 1983. Light and Color in Nature and Art, first ed. Wiley.

Yuan, X., Liu, Y.C., Yuen, D.A., Pergler, T., Chen, B., Shi, Y., 2007. An efficient system for creating synthetic insar images from simulations. Pure Appl. Geophys. (PAGEOPH), Birkhauser, Verlag AG.

Yuan, X., Nguyen, M.X., Chen, B., Porter, D.H., 2005. High dynamic range volume visualization. In: Proc. of IEEE Visualization'05, pp. 327–334.

Yuan, X., Nguyen, M.X., Chen, B., Porter, D.H., July/August 2006. HDRVolVis: high dynamic range volume visualization. IEEE Trans. Visual. Comput. Graph. 12 (4), 433–455.